Supporting Information for

"Subduction initiation with vertical lithospheric heterogeneities and new fault formation"

Xiaolin Mao[1], Michael Gurnis[1], Dave A. May[2]

[1]Seismological Laboratory, California Institute of Technology, Pasadena, CA, 91125, USA

[2]Department of Earth Sciences, University of Oxford, Oxford, United Kingdom

Contents

Method details

Surface process

To incorporate the influence of surface processes on subduction zone evolution, we consider a simple 2D law of topographic changes that could simulate erosion and sedimentation at the scale of several tens of kilometers [*Avouac and Burov*, 1996]. Assuming the rate of downslope transport of debris, q_e, is proportional to the local slope, we have

$$q_e = -k\frac{\partial h}{\partial x}, \tag{1}$$

where k is the mass diffusivity coefficient. From the mass conservation law, h obeys

$$\frac{\partial h}{\partial t} = -\frac{\partial q_e}{\partial x}. \tag{2}$$

With constant k, equations (1) and (2) lead to the linear diffusion equation

$$\frac{\partial h}{\partial t} = k\frac{\partial^2 h}{\partial x^2}. \tag{3}$$

Equation (3) is applied to the free surface between time steps and after the topography updating related to subsurface dynamics. A layer of sediment tracers are added on the free surface before applying Eq. (3). These sediment tracers become out of the model domain

Corresponding author: Xiaolin Mao, xlmao@gps.caltech.edu

and are deleted in the erosion region after the topographic changes, while they survive at the sedimentation region. The mass diffusivity coefficient is set to be 2×10^4 m^2/yr in our model [Mao et. al., manuscript in preparation].

Phase change

Discrete 4D (temperature, pressure, rock type and total water content) phase maps for density and free water content are calculated using Perplex [*Connolly*, 2005] and stored for lookup during the computation. Four rock types are considered: pyrolite, harzburgite (only in case SI8), basalt and sediment. The ranges of temperature and pressure cover the whole upper mantle. The total water content varies from 0 to 10-20 percent. During the computation, rock type and total water content are recorded on tracers, and temperature and pressure are obtained from solution of the numerical model. After each Stokes solve, density and free water content on a tracer are updated through refer to stored phase maps for the corresponding rock type. Linear interpolation is used to obtain the value between adjacent nodes of temperature, pressure and total water content [Mao et. al., manuscript in preparation].

Elastic Viscous Stress Splitting (EVSS)

In our models, we employ the Elastic Viscous Stress Split (EVSS) visco-elastic model [*Keunings*, 2000]. The EVSS model is built upon the following deviatoric stress decomposition

$$\boldsymbol{\tau} = 2\eta_v \dot{\boldsymbol{\varepsilon}}(\boldsymbol{u}) + \boldsymbol{\tau}_e, \tag{4}$$

where η_v is the viscosity of the purely viscous component, $\dot{\boldsymbol{\varepsilon}}(\boldsymbol{u})$ is the strain rate tensor, and $\boldsymbol{\tau}_e$ is the visco-elastic contribution to the stress tensor. The visco-elastic stress $\boldsymbol{\tau}_e$ evolves according to the following

$$\boldsymbol{\tau}_e + \frac{\eta_e}{G}\left(\frac{D\boldsymbol{\tau}_e}{Dt} + \boldsymbol{J}(\boldsymbol{u}, \boldsymbol{\tau}_e)\right) = 2\eta_e \dot{\boldsymbol{\varepsilon}}(\boldsymbol{u}), \tag{5}$$

where η_e and G are the viscosity and shear modulus of the elastic component of the stress respectively, and $\frac{D\boldsymbol{\tau}_e}{Dt} + \boldsymbol{J}(\boldsymbol{u}, \boldsymbol{\tau}_e)$ is the Jaumann corotational stress rate, where

$$\boldsymbol{J}(\boldsymbol{u}, \boldsymbol{\tau}_e) = \boldsymbol{\tau}_e \boldsymbol{W} - \boldsymbol{W}\boldsymbol{\tau}_e, \tag{6}$$

and

$$W_{ij} = \frac{1}{2}\left(\frac{\partial u_i}{\partial x_j} - \frac{\partial u_j}{\partial x_i}\right). \tag{7}$$

The partition of the total viscosity is given by

$$\eta = (1 - \phi)\eta_v + \phi\eta_e, \quad \phi \in [0, 1], \tag{8}$$

where η is the conventional viscosity, and ϕ is the partition coefficient. ϕ decreases linearly from close 1 in the lithosphere to 0 in the asthenosphere with increasing temperature, which results visco-elastic and viscous behaviors in the two regions respectively. When ϕ is set to 1, the EVSS formulation reverts back to the visco-elastic model commonly used in geodynamics [e.g., *Moresi et al.*, 2003]. The benefit of using EVSS model is that when time step continuously decreases, $\boldsymbol{\tau}$ converges to the stress from the purely viscous part, which helps to stabilize numerical simulation [Mao et. al., manuscript in preparation].

References

Avouac, J.-P., and E. Burov (1996), Erosion as a driving mechanism of intracontinental mountain growth, *Journal of Geophysical Research: Solid Earth*, *101*(B8), 17,747–17,769, doi:10.1029/96JB01344.

Connolly, J. A. (2005), Computation of phase equilibria by linear programming: a tool for geodynamic modeling and its application to subduction zone decarbonation, *Earth and Planetary Science Letters*, *236*(1), 524–541, doi:10.1016/j.epsl.2005.04.033.

Keunings, R. (2000), Advances in the computer modeling of the flow of polymetric liquids, *Computational Fluid Dynamics Journal*, *9*(1), 449–458.

Moresi, L., F. Dufour, and H.-B. Mühlhaus (2003), A lagrangian integration point finite element method for large deformation modeling of viscoelastic geomaterials, *Journal of Computational Physics*, *184*(2), 476–497.

Tables

Table S1. Thermal and rheological parameters

Parameter	Value
surface temperature	0 °C
bottom temperature	1400 °C
thermal diffusivity (κ)	10^{-6} m^2 s^{-1}
maximum viscosity cutoff (η_{max})	10^{24} Pa s
minimum viscosity cutoff (η_{min})	10^{18} Pa s
shear modulus (G)	30 GPa
maximum yield stress (τ_{yield})	150 MPa
initial water content in mantle	100 ppm
preexponential factor in mantle (A_m)	1.6 x 10^{-15} Pa^{-n} s^{-1}
exponent in mantle (n_m)	3.2
activation energy in mantle (E_m)	540 kJ mol^{-1}
initial water content in crust	2.68%
preexponential factor in crust (A_c)	2 x 10^{-23} Pa^{-n} s^{-1}
exponent in crust (n_c)	3.2
activation energy in crust (E_c)	238 kJ mol^{-1}
initial water content in sediment	7.29%
preexponential factor in sediment (A_s)	5 x 10^{-21} Pa^{-n} s^{-1}
exponent in sediment (n_s)	2.3
activation energy in sediment (E_s)	154 kJ mol^{-1}

Table S2. Table of models. WZ is short for weak zone.

Model	WZ dip angle	WZ width	Harzburgite layer
SI1	90°	10 km	No
SI2	30°	10 km	No
SI3	45°	10 km	No
SI4	60°	10 km	No
SI5	75°	10 km	No
SI6	90°	15 km	No
SI7	90°	5 km	No
SI8	90°	10 km	15 km

Figures

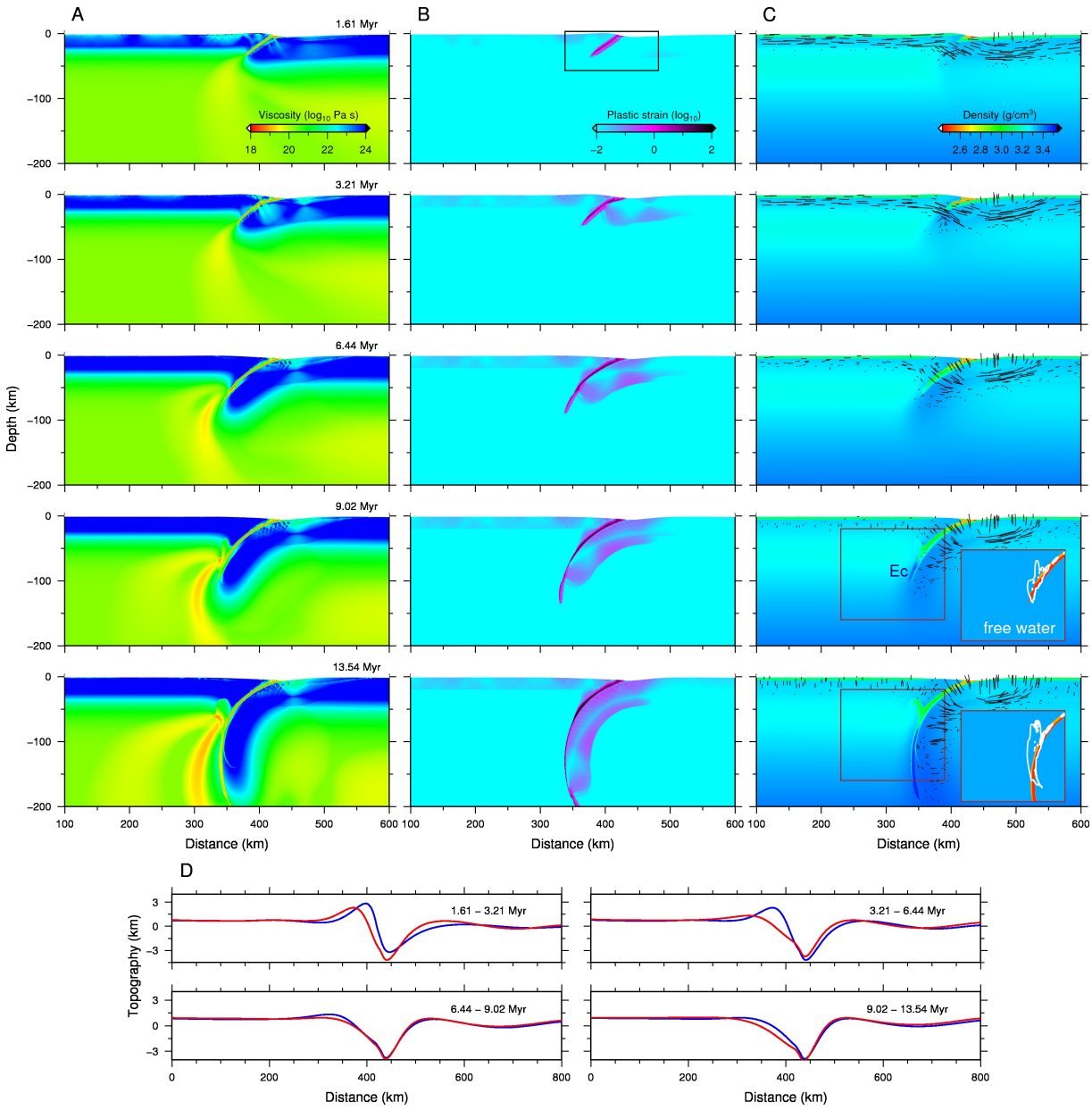

Figure S1. Model results (case SI2). (a) Effective viscosity evolution. (b) Accumulation of plastic strain. The black box shows the corresponding region for Figure 4b. (c) Density evolution. Black lines show direction and magnitude of maximum principal stress. Rock types and free water contents are shown in the insets with different colors and white contours. (d) Topography changes. Blue and red lines show initial and final topography for each time interval.

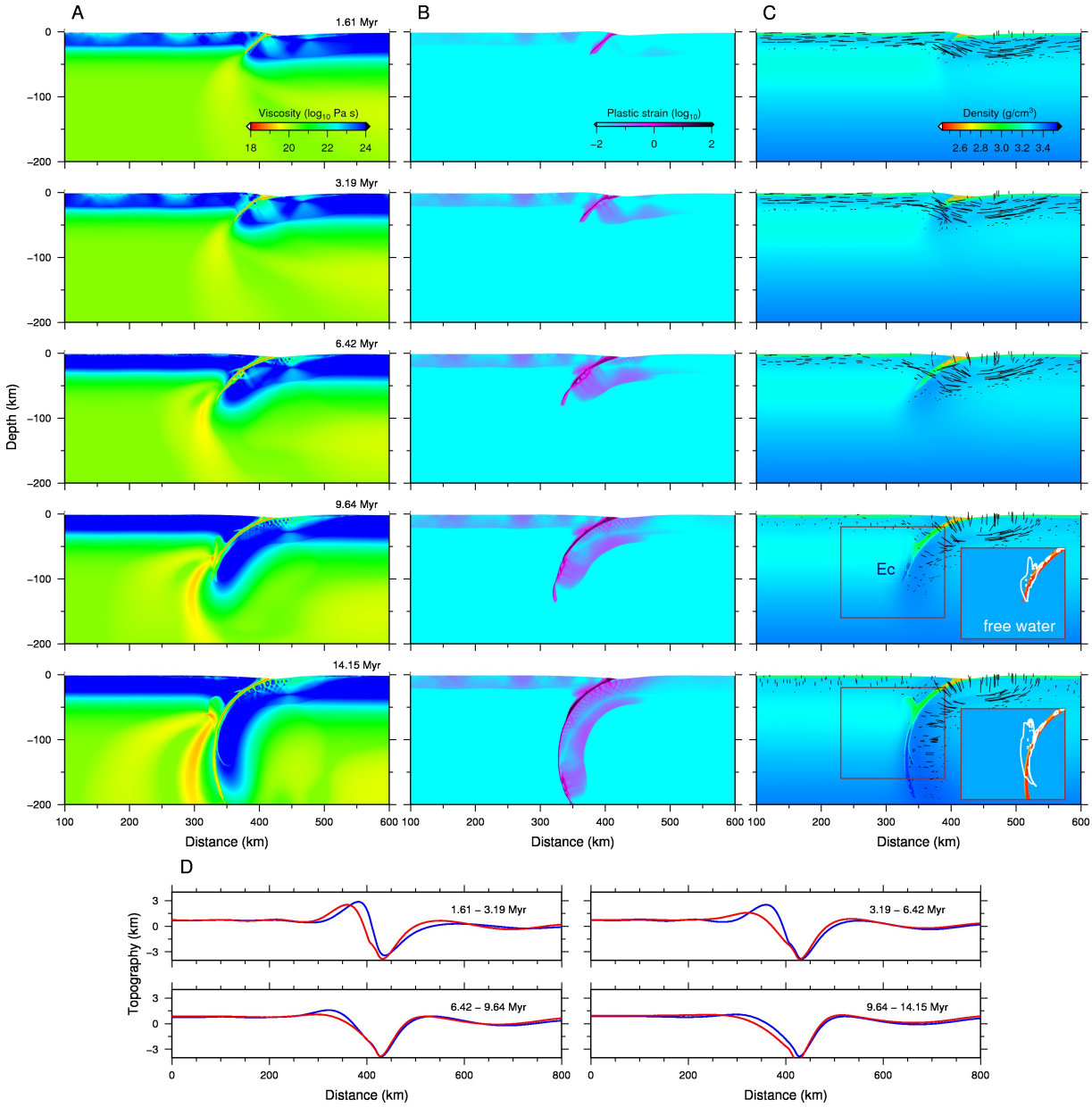

Figure S2. Model results (case SI3). (a) Effective viscosity evolution. (b) Accumulation of plastic strain. (c) Density evolution. Black lines show direction and magnitude of maximum principal stress. Rock types and free water contents are shown in the insets with different colors and white contours. (d) Topography changes. Blue and red lines show initial and final topography for each time interval.

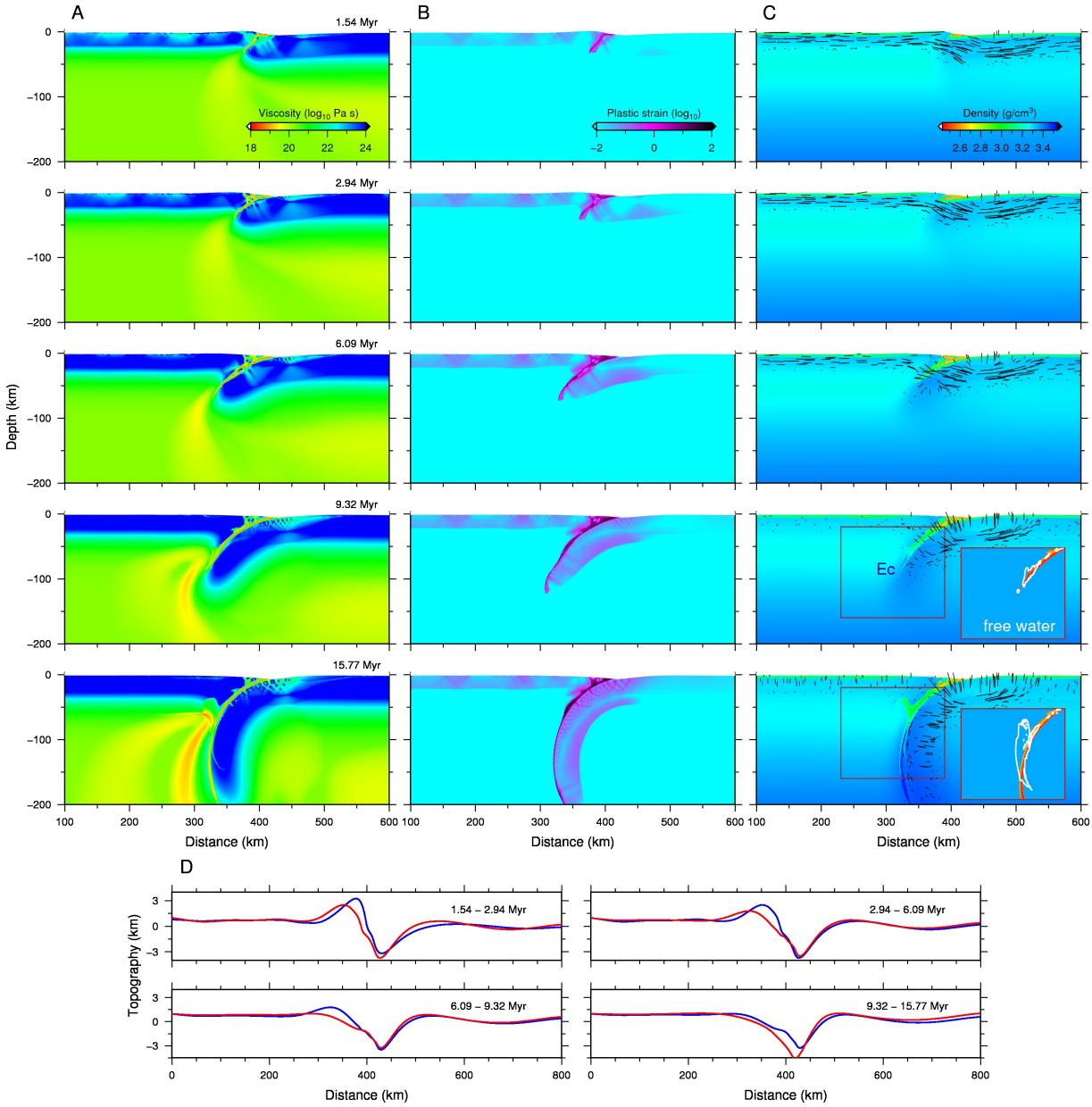

Figure S3. Model results (case SI4). (a) Effective viscosity evolution. (b) Accumulation of plastic strain. (c) Density evolution. Black lines show direction and magnitude of maximum principal stress. Rock types and free water contents are shown in the insets with different colors and white contours. (d) Topography changes. Blue and red lines show initial and final topography for each time interval.

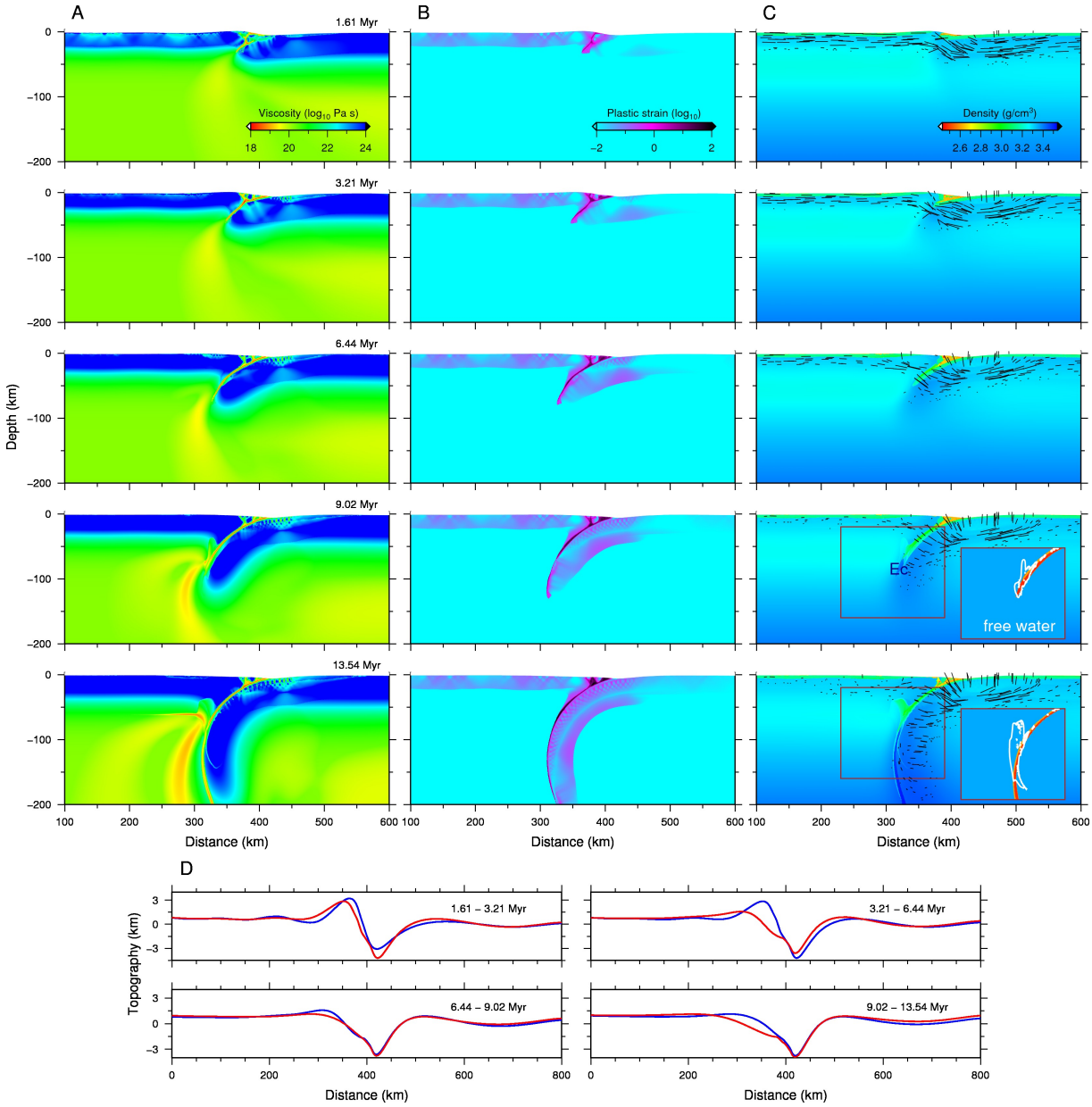

Figure S4. Model results (case SI5). (a) Effective viscosity evolution. (b) Accumulation of plastic strain. (c) Density evolution. Black lines show direction and magnitude of maximum principal stress. Rock types and free water contents are shown in the insets with different colors and white contours. (d) Topography changes. Blue and red lines show initial and final topography for each time interval.

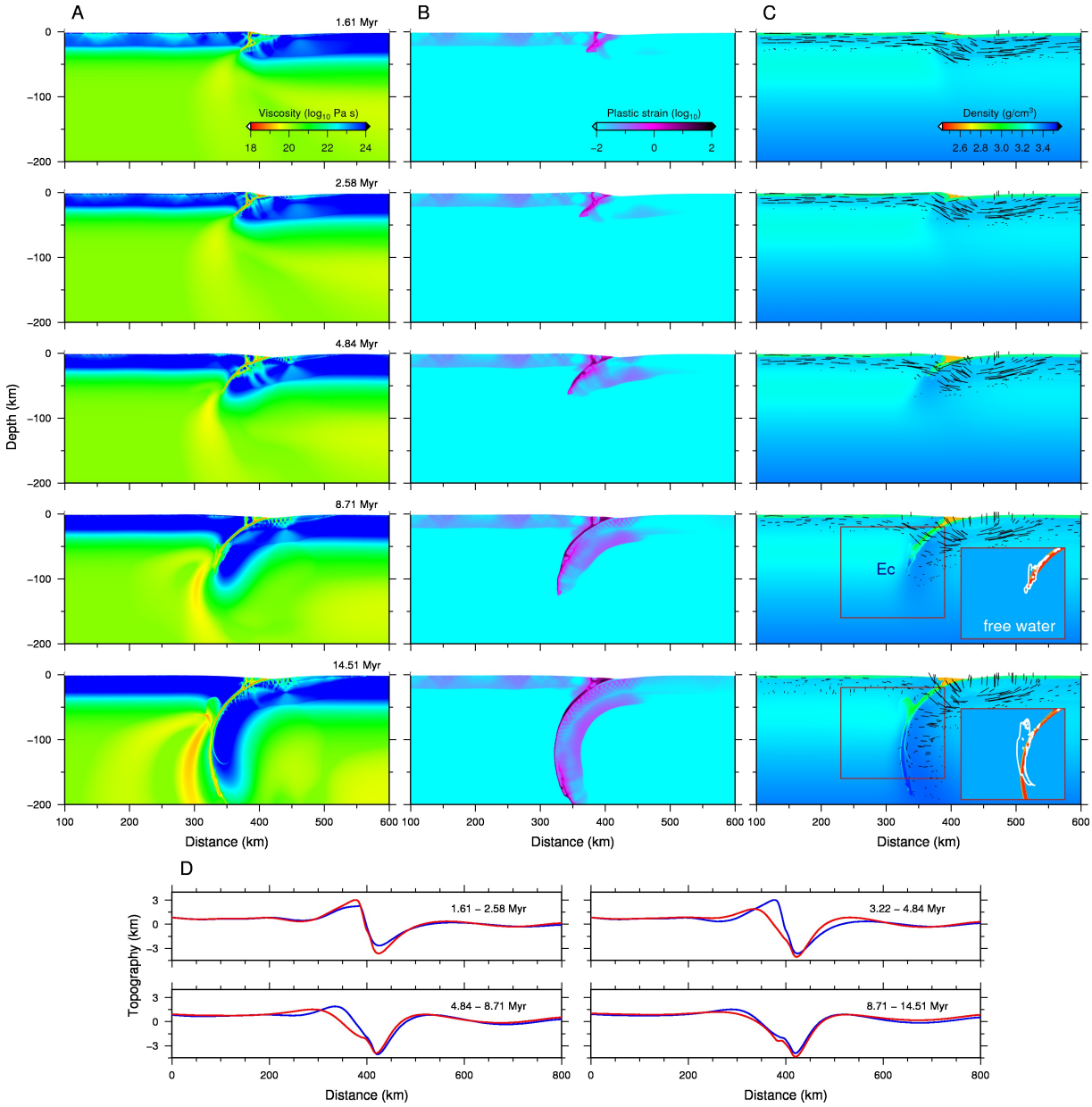

Figure S5. Model results (case SI6). (a) Effective viscosity evolution. (b) Accumulation of plastic strain. (c) Density evolution. Black lines show direction and magnitude of maximum principal stress. Rock types and free water contents are shown in the insets with different colors and white contours. (d) Topography changes. Blue and red lines show initial and final topography for each time interval.

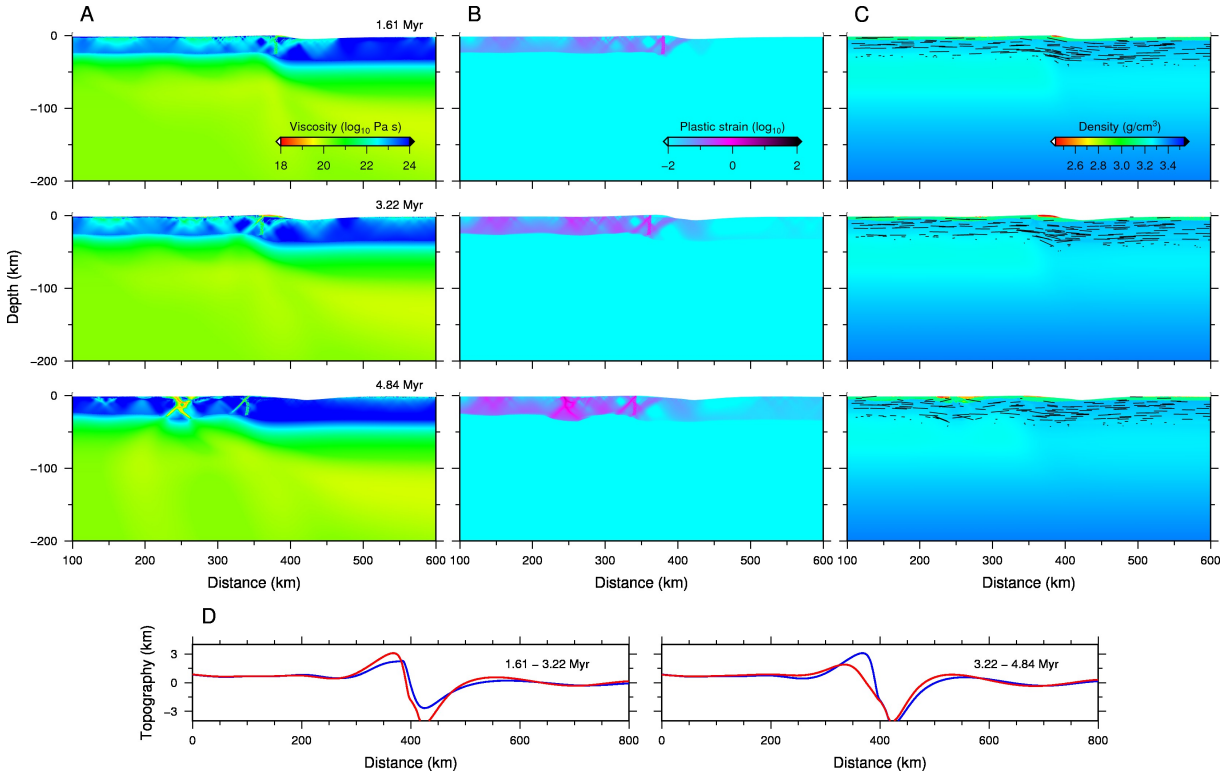

Figure S6. Model results (case SI7). (a) Effective viscosity evolution. (b) Accumulation of plastic strain. (c) Density evolution. Black lines show direction and magnitude of maximum principal stress. (d) Topography changes. Blue and red lines show initial and final topography for each time interval.

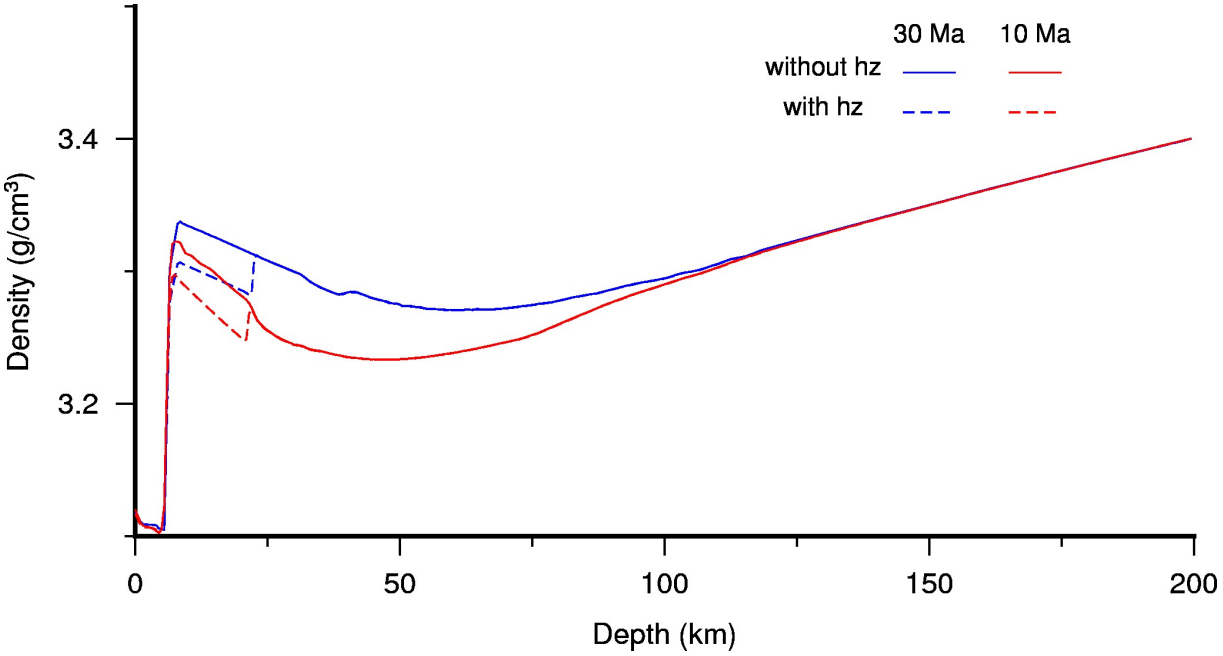

Figure S7. Along depth variation of initial density structure. hz: harzburgite.

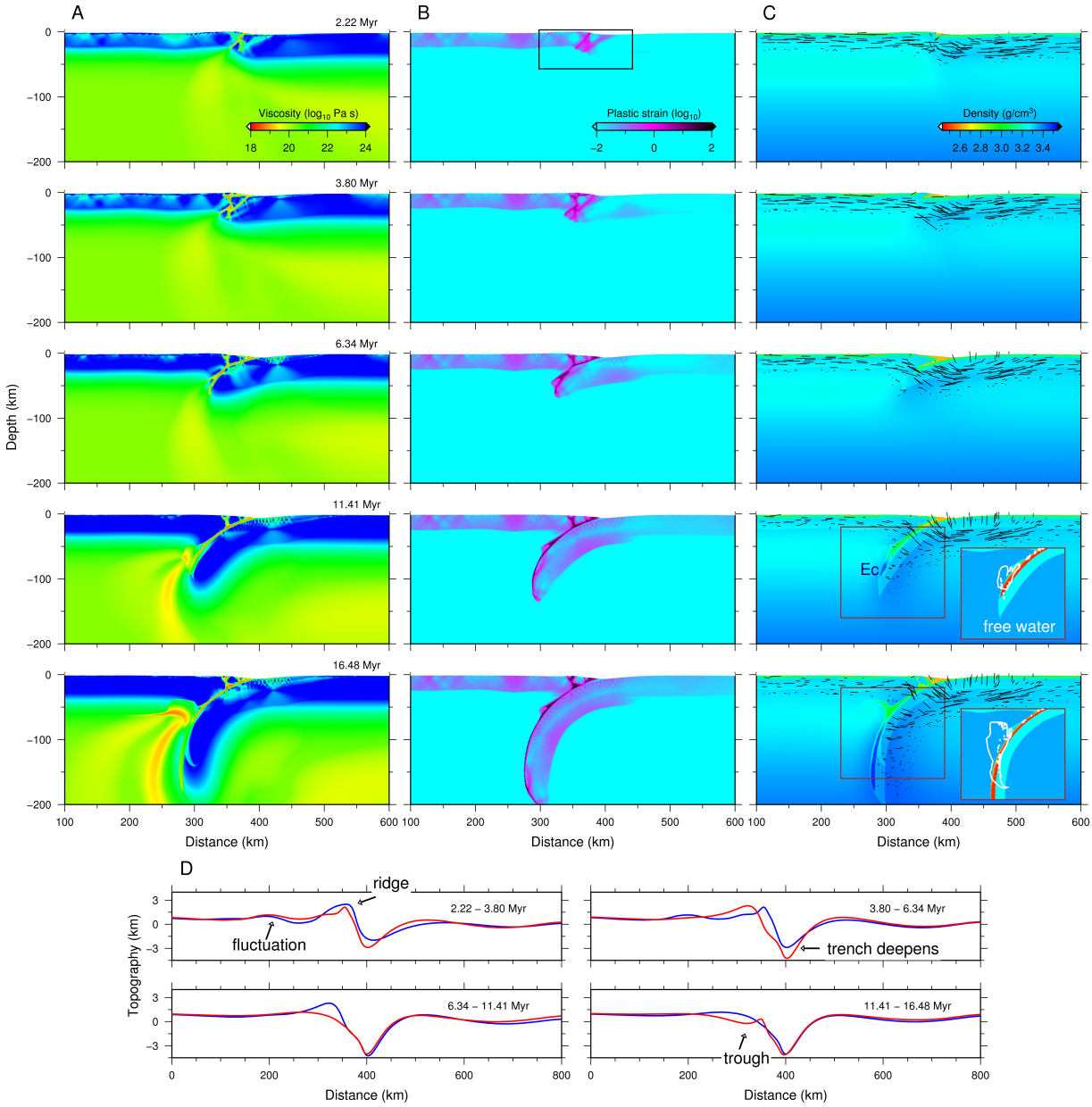

Figure S8. Model results of a case with a 15 km Harzburgite layer (case SI8). (a) Effective viscosity evolution. (b) Accumulation of plastic strain. (c) Density evolution. Black lines show direction and magnitude of maximum principal stress. (d) Topography changes. Blue and red lines show initial and final topography for each time interval.